LA-UR-21-30756
Approved for public release; distribution is unlimited.

Title: R-CERT Project Analysis Report

Author(s): Lum, Sheera Shelby

Intended for: Report

Issued: 2021-10-28

R-CERT Project

Analysis Report

Sheera S. Lum

LA-UR-21-xxxx
October 13, 2021

Derivative Classifier Review
Reviewed and determined to be UNCLASSIFIED. This review does not constitute clearance for public release.
Derivative Classifier
Name/Z#/Org: DC name/DC Z#/DC org
Signature/Date:
Derived from: DC derived

Los Alamos
NATIONAL LABORATORY

Prepared for: U.S. Department of Energy/National Nuclear Security Administration,
Los Alamos Field Office
NameTitle
Org

Prepared by: NameTitle
Org

Approvals:

Name	Title	Signature	Date

Contents

Figures

Contents

Tables

Abstract

The R-CERT project aims to determine if PBX 9501 will experience a deflagration to detonation transition (DDT) while in a high pressure environment. Combined efforts in design and analysis between multiple groups at Los Alamos National Laboratory (LANL) were required to finalize the test design. The proposed design of the case assembly (i.e. the pressure vessel that would contain the high explosive) was analyzed and iteratively modified until modeling efforts predicted the case would maintain pressure up to 5000 *psi* under quasi-static conditions. To prevent the case from being excessively robust beyond its design requirement, grooves were added to the case geometry with depths and radii of 4 *mm*, thus weakening the case while maintaining much of the mass of the proposed design.

1 Introduction

This report outlines the analysis efforts performed by the Advanced Engineering Analysis Group (W-13) for the R-CERT project, which aims to determine if confined PBX 9501 will go through a deflagration to detonation transition (DDT) by encasing the high explosive (HE) in a pressure vessel. W-13 efforts included building a representative model of the proposed geometry to aid in the iterative design process in collaboration with the Explosive Applications and Special Projects Group (M-6) and the Weapon Systems Safety Analysis Group (W-10). Geometry was provided by M-6, and W-13 aided in providing recommendations for any design changes. An axisymmetric model was created from the assembly design, investigating the behavior of the testbed when under quasi-static loading conditions.

2 Case: Assembly and Design

The assembly design for the case consists of three main parts: upper and lower halves of the case and four (4) clamps designed to seal the case up to 5000 *psi*. Both made from 316 Stainless Steel (SS 316), the two halves of the case are nearly geometrically identical, differing primarily at the clamping joint. The four clamps are each geometrically equivalent and composed of Alloy 17-4PH H900 Stainless Steel (SS 17-4PH H900). An isometric cutaway of the case can be seen in Figure 2-1. Though not included for this analysis, each of the clamps will be fastened together with steel bolts.

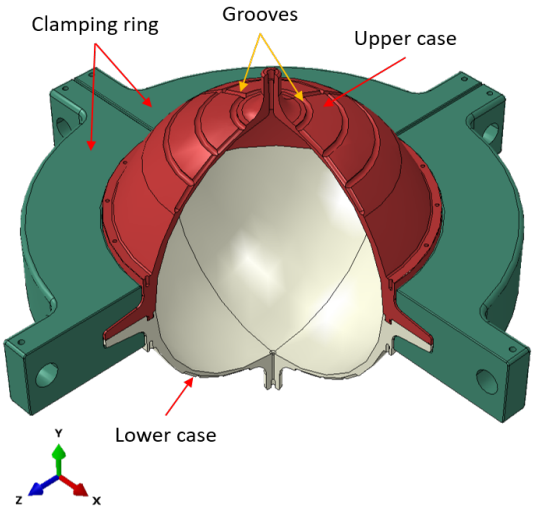

Figure 2-1: Isometric cutaway view of the case assembly. The latitudinal rings grooved into the upper case were included with the design intent of weakening the pressure vessel while still maintaining its inertial confinement capabilities; less visible are longitudinal lines that serve this same purpose.

The idealized version of the case would be a hermetically sealed sphere in which the two halves are welded together post-assembly. With the presence of high explosive in the assembly, welding was not a viable option because of safety concerns. As an alternative, the clamping ring was integrated to strengthen the case joint. Two O-ring grooves, which can be seen in Figure 2-3, were also added to the upper case to further mitigate leakage between the two halves. The final design was achieved by modifying the design until the analysis results aligned with the predefined design metric.

2.1 Geometry

The geometry for both the case subassembly (i.e. upper and lower halves) and clamping ring was supplied by M-6 as STEP files. All geometric dimensions were converted to be consistent with the International System of Units ($mm - N - s$).

2.1.1 Case Subassembly

Taking advantage of the largely symmetric case geometry, an axisymmetric model was used for executing the analysis. Placing the reference coordinate system origin at the spherical center as shown in Figure 2-2(a), the axisymmetric geometry consisted of the case profile coinciding with the

X-Y plane as depicted in Figure 2-2(b).

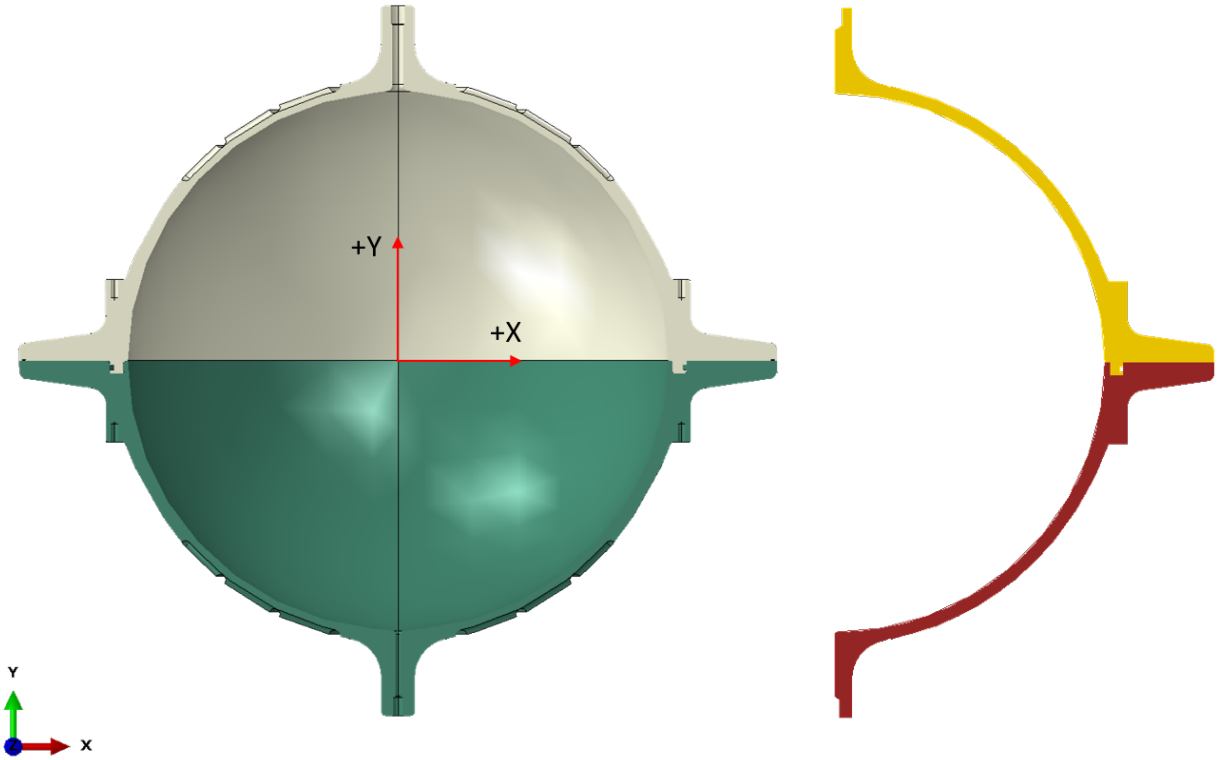

Figure 2-2: From left to right: (a) A cross-section of the spherical vessel. (b) The axisymmetric representation of the case geometry.

Figure 2-2(a) displays a cross-section of the case subassembly through the X-Y plane, which passes through the reference coordinate system (i.e., the center of the sphere). The positive z-axis points outside of the page. Figure 2-2(b) shows the axisymmetric representation of the case geometry. The geometry is axisymmetric because the original three-dimensional (3D) representation can be completely restored by revolving the geometry 360 degrees about the y-axis (symmetry axis).

To obtain axisymmetric geometry, all non-axisymmetric features were omitted using CUBIT meshing software. This included the alignment holes (shown in Figure 2-3) as well as all longitudinal and latitudinal[1] groove features. The purpose of the grooves was to weaken the geometry enough to prevent the case from being too strong while simultaneously preserving the overall inertial mass. The outermost O-ring groove, shown in Figure 2-3, was also omitted because it was a design feature that was added in after analysis was already complete.

The geometry was further simplified by omitting chamfers, fillets, and any other features that did not directly contribute to the structural integrity of the parts. The holes aligned with the symmetry axis were removed because they will be filled with an epoxy once assembly is complete.

[1] Although the latitudinal grooves are axisymmetric, the geometry for both latitudinal and longitudinal grooves was determined in a separate analysis as described in Section 4.1.

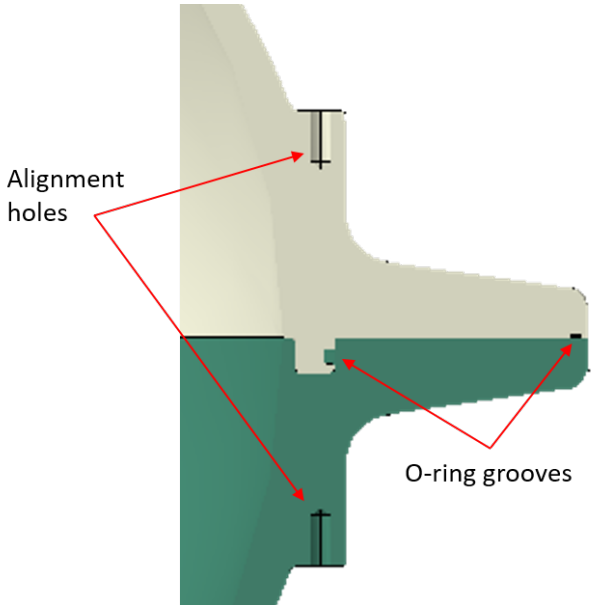

Figure 2-3: Alignment holes (the pattern of which is depicted in Figure 2-1 for the upper case) and O-ring grooves. The outermost groove feature was added in after analysis efforts were already complete.

2.1.2 Clamping Ring

Like the case subassembly, CUBIT meshing software was used to manipulate and mesh the clamping ring geometry. To streamline the process, M-6 provided geometry for the clamping ring with the bolted joints omitted[2], thus forming an idealized ring representation of the clamp as shown in Figure 2-4(a). The axisymmetric geometry could then be extracted from the part cross-section to obtain the result shown in Figure 2-4(b).

Besides the bolted joints, filleted features that did not contribute to the structural makeup of the part were also omitted. Features that interfaced with the upper and lower case components were left untouched.

[2]The strength of the bolted joints was investigated by M-6. Bolts were selected with a rating of 50 *ksi*, which is ten times the strength required for the case assembly. Thus, the bolted joints were not considered as a failure mode by W-13 given the high strength capacity of the bolts.

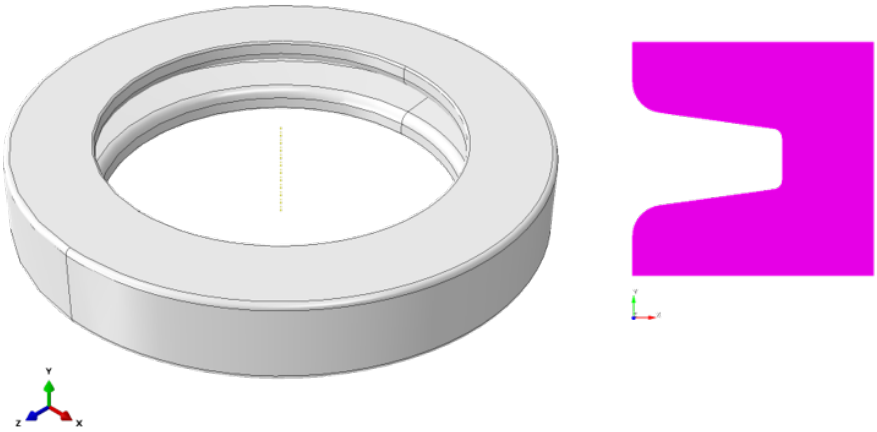

Figure 2-4: From left to right: (a) Defeatured clamping ring provided by M-6. (b) Cross-sectional view of clamping ring, which can be used, in combination with the radial distance from the symmetry axis, to fully restore the original 3D geometry.

2.2 Mesh

2.2.1 Case Subassembly

Given their overlapping interfaces and nearly identical geometry, the upper and lower case components were meshed concurrently in CUBIT to promote similar meshing between the two parts. The subassembly was divided into four equivalent sections as shown in Figure 2-5(a), followed by deleting three of the four sections and defeaturing the remaining geometry to obtain the representation shown in Figure 2-5(b).

The case geometry was further prepped for meshing by partitioning the geometry as shown in Figure 2-5(c). Partitioning not only improves the mesh quality but also eliminates the need for using an unstructured mesh, which can be lower in quality and computationally more expensive. All partitioned volumes were imprinted and merged with their respective parts. Imprinting ensures all nodes associated with a single part will align across the partitioned regions, while merging removes redundant nodes that arise from partitioning.

After partitioning, the two-dimensional (2D) axisymmetric geometry described in Figure 2-2(b) was preserved, while all other geometry shown in Figure 2-5(c) was deleted. A global seed size of 1 mm was applied to the model, and a mesh density of six elements across the case thickness was used. Although a mesh convergence study indicated that four elements through the thickness was sufficient for capturing bending effects, the low computational intensity of an axisymmetric model justified the higher mesh density. After simultaneously meshing the upper and lower case geometry, each meshed part was independently exported as an Abaqus input file for use in later analysis. The final meshed geometry for the case subassembly can be seen in Figure 2-6.

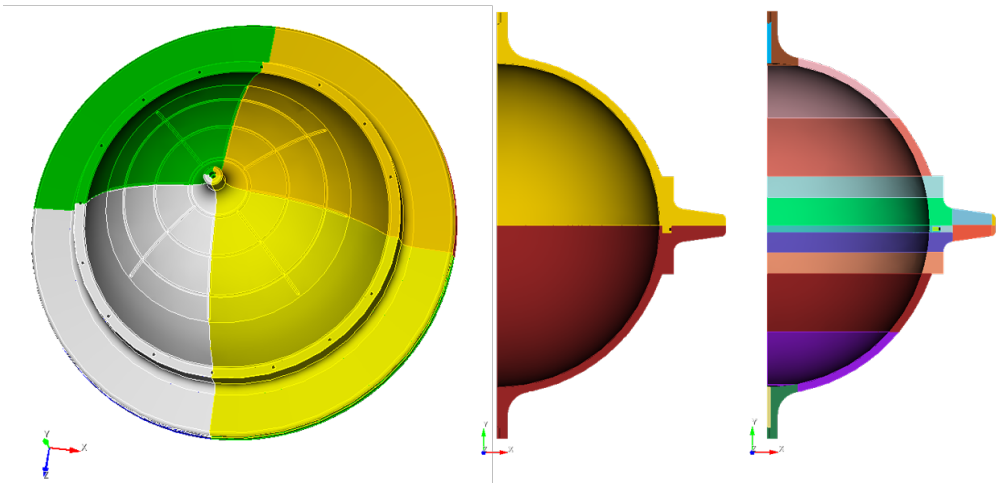

Figure 2-5: From left to right: (a) A top-down view of the upper case after dividing it into four geometrically identical sections. The green, white, and yellow sections were omitted prior to partitioning the geometry. A similar process was simultaneously executed on the lower half of the case. (b) The defeatured geometry after removing three of the four sections depicted in (a). (c) The partitioned case geometry.

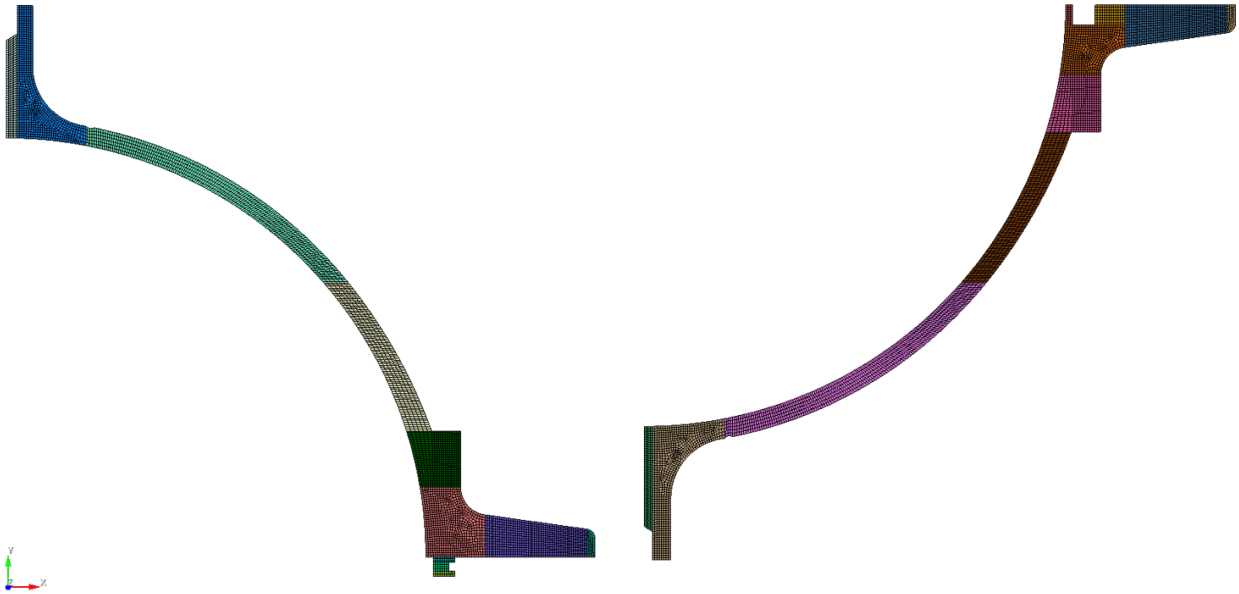

Figure 2-6: The 2D meshed geometry for the upper (left) and lower case components.

2.2.2 Clamping Ring

While a 2D mesh was applied to the case, the clamping ring was meshed in a three-dimensional state prior to isolating the axisymmetric geometry shown in Figure 2-4(b). To mesh the clamping ring, the geometry in Figure 2-4(a) was divided into four geometrically equivalent sections, deleting all but one as shown in Figure 2-7(a). After selectively partitioning, imprinting, and merging the geometry as shown in Figure 2-7(b), the part was meshed with a global seed size of 1 mm, which is consistent with the mesh seed size used for the case subassembly. The mesh associated with the axisymmetric geometry, which can be seen in Figure 2-7(c), was exported as an Abaqus input file, where the nodal locations are based on the clamping ring location in the case assembly.

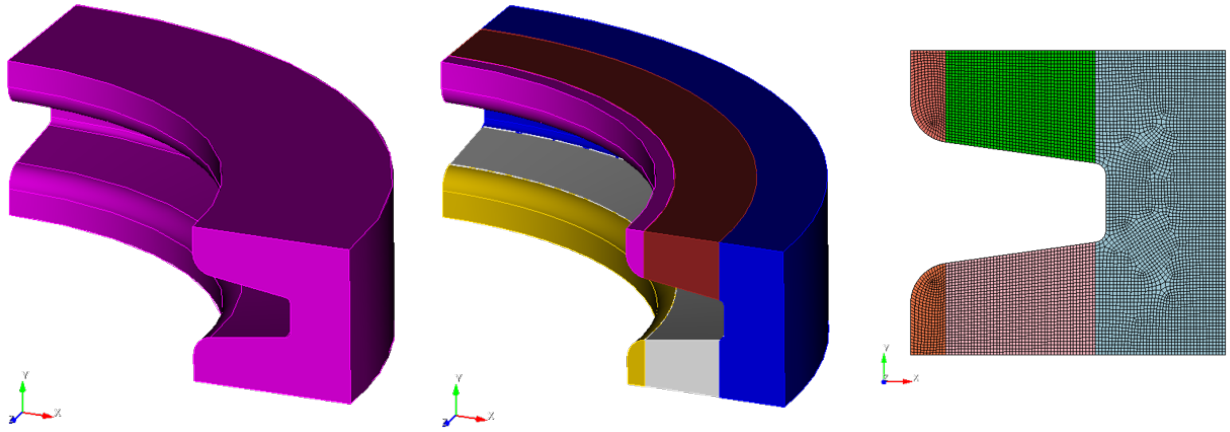

Figure 2-7: From left to right: (a) Quarter representation of the geometry from Figure 2-4(a). If this geometry was reflected twice (once about the X-Y plane and again about the Y-Z plane), the original geometry would be restored. (b) The partitioned geometry of the clamping ring. (c) The meshed axisymmetric geometry of the clamping ring, which was extracted from the 3D mesh applied to the geometry in (b).

Because CUBIT does not have the option to select an axisymmetric-compatible element type, the input files for each part were manually modified after export, redefining each mesh to have continuum 4-node bilinear axisymmetric elements with reduced integration and hourglass control (CAX4R). Reassigning element type had no effect on the original geometric mesh quality.

2.3 Material

The material assigned to the upper and lower case components was SS 316. Because M-6 was also contributing their own analytical efforts, identical material properties were used between W-13 and M-6 for the upper and lower case. Parameters for the material model were provided by M-6 and were found to be comparable to those available in the Granta Material Database. The material properties used for the case subassembly were placed in Table 2-1.

Table 2-1: Material properties for the case assembly

Material	Density $\frac{lb}{in^3}$ ($\frac{tonne}{mm^3}$)	Young's Modulus $10^3 ksi$ (MPa)	Poisson's Ratio	Yield Stress ksi (MPa)	UTS ksi (MPa)	Source
SS 316	0.2783 (7.952E-09)	28.1 (193743)	0.26	41.62 (286.9)	142.3 (980.9)	All values taken from [3] except for Yield and UTS, which were taken graphically from [2].
SS 17-4PH H900	0.2822 (7.81E-09)	28.6 (197000)	0.26	169.7 (1170)	190.0 (1310)	[1]

SS 17-4PH H900, shown in Table 2-1, was determined to be a viable material for the clamping ring given its high strength. The material model selected for the clamping ring was similar to that of SS 316 with the exception of having a much higher yield strength and ultimate tensile strength (UTS). The decision to select a material that deviated from that of the case subassembly was due to prior analytical results revealing that the clamping joint between the sphere and the ring would not be strong enough to maintain a hermetic steel if all components were made from SS 316.

2.4 Loading and Boundary Conditions

As shown in Figure 2-8, nodes coincident with the symmetry axis were fixed in the radial direction to prevent any non-physical lateral translations (i.e. translations in the x-direction). Additionally, a region of nodes along the base of the clamping ring were fixed along the axial direction (i.e. y-direction) to fully constrain the model. Constraining motion in the y-direction prevents excessive vertical translation in space.

A uniform pressure load was applied to the internal case surface as shown in Figure 2-8 and was applied linearly over the course of the analysis step. Because the goal of the study was to determine the maximum pressure the case could withstand, a linear pressure function was used as represented in Figure 2-9, requesting plastic equivalent strain (PEEQ) output during the analysis at 1 MPa increments.

Case: Assembly and Design

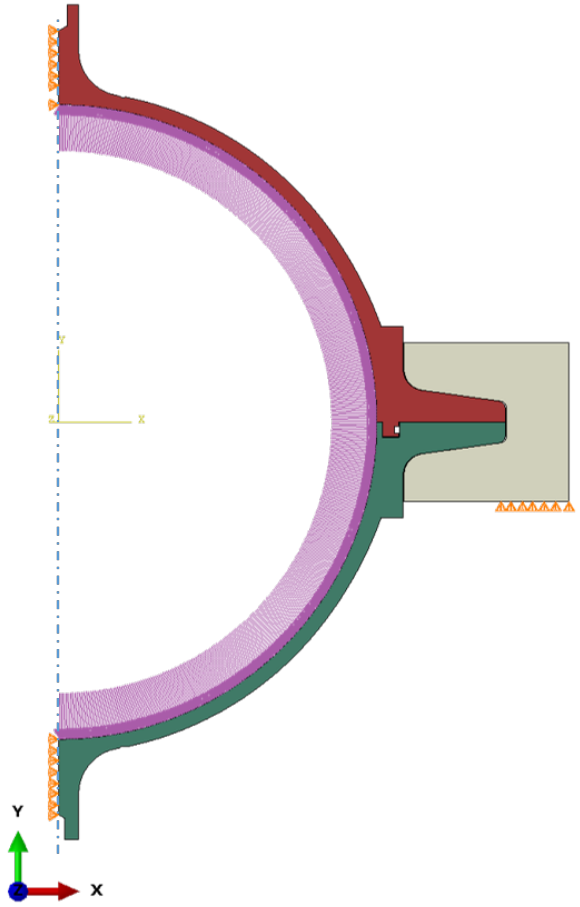

Figure 2-8: Loading conditions and boundary conditions for the case assembly (mesh hidden for clarity). All nodes coincident with the symmetry axis were fixed in the radial (horizontal) direction (as indicated by the orange arrows pointing to the right). A region of nodes at the base of the clamping ring were fixed in the axial (vertical direction) to keep the model stationary. The arrows shown in pink denote the uniform load applied to the internal case surface.

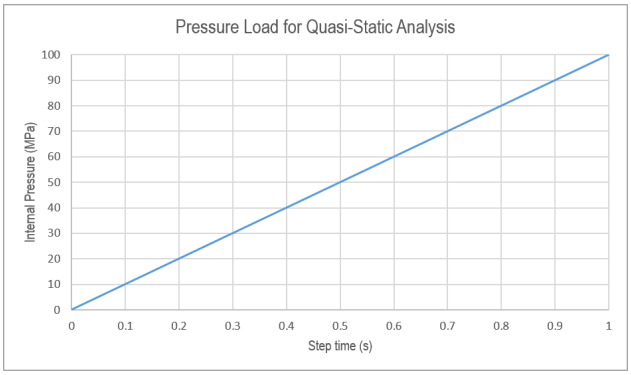

Figure 2-9: Linear function definition for applying internal pressure load to case. A wide pressure range was used to ensure the point of failure was captured.

2.5 Interactions

A general contact definition was applied to the model, using a Penalty frictional formulation for tangential behavior. A tangential frictional coefficient of 0.7 was assigned to the contact property definition, which is a frictional value on par with that typically used for steel-on-steel contact [4].

3 Case: Analysis and Results

A quasi-static Dynamic, Implicit analysis step was used for applying the pressure load, accounting for geometric nonlinearity. Because the application of the step was defined as quasi-static, the amount of time over which the step occurred was of no consequence. Thus, 1 second was conveniently chosen for the step duration.

During the pressure loading step, the internal pressure function was applied linearly for the step duration. Failure of the case assembly was attributed to lack of model convergence (i.e. aborting the analysis prior to reaching 100 MPa) (14.5 ksi). Because the clamping joint was anticipated to be the weakest region, verifying that the O-ring hermetic seal was sustained up to 5000 psi (34.5 MPa) was also of concern.

The analysis successfully converged until exceeding 54 MPa (7832 psi), which is well beyond the 5000 psi design requirement. To examine whether the clamping joint remained sufficiently sealed up to the design pressure, the output was visualized at 36 MPa (5221 psi) as shown in Figure 3-1(a). At this internal pressure, the O-ring groove remained seated within the groove of the lower case (see Figure 3-1(b)). Thus, given quasi-static conditions, the O-ring at this groove should maintain a complete seal up to the design pressure.

Additionally, the PEEQ and Von Mises stresses were examined. Figure 3-1(a) shows that the PEEQ at 36 MPa internal pressure did not exceed 13 % at any location within the model, which is well below the plastic strain at UTS for both the case subassembly and clamping ring materials. At the clamping joint, PEEQ is zero virtually everywhere as indicated in Figure 3-1(b), while the maximum value occurs at the top and bottom latitudinal grooves of the upper and lower case components. This outcome supports the presumption that the case subassembly will fail prior to the joint. It should be noted that these grooves are significantly smaller than those included in the final design, which is why the case subassembly withstands an internal pressure well beyond 5000 psi during this analysis.

As a final assurance of the joint strength, the stresses seen in Figure 3-1(c) show good agreement with the PEEQ output in that yielding is very small at the joint. Given that the yield stress of SS 17-4PH is 1170 MPa, yielding was just starting to occur within the clamping ring at an internal pressure of 36 MPa.

In Section 4.2, the groove depth geometry required to sufficiently weaken the case is discussed. The results from the both the clamping joint and groove geometry analyses were combined to provide an overall design recommendation to M-6.

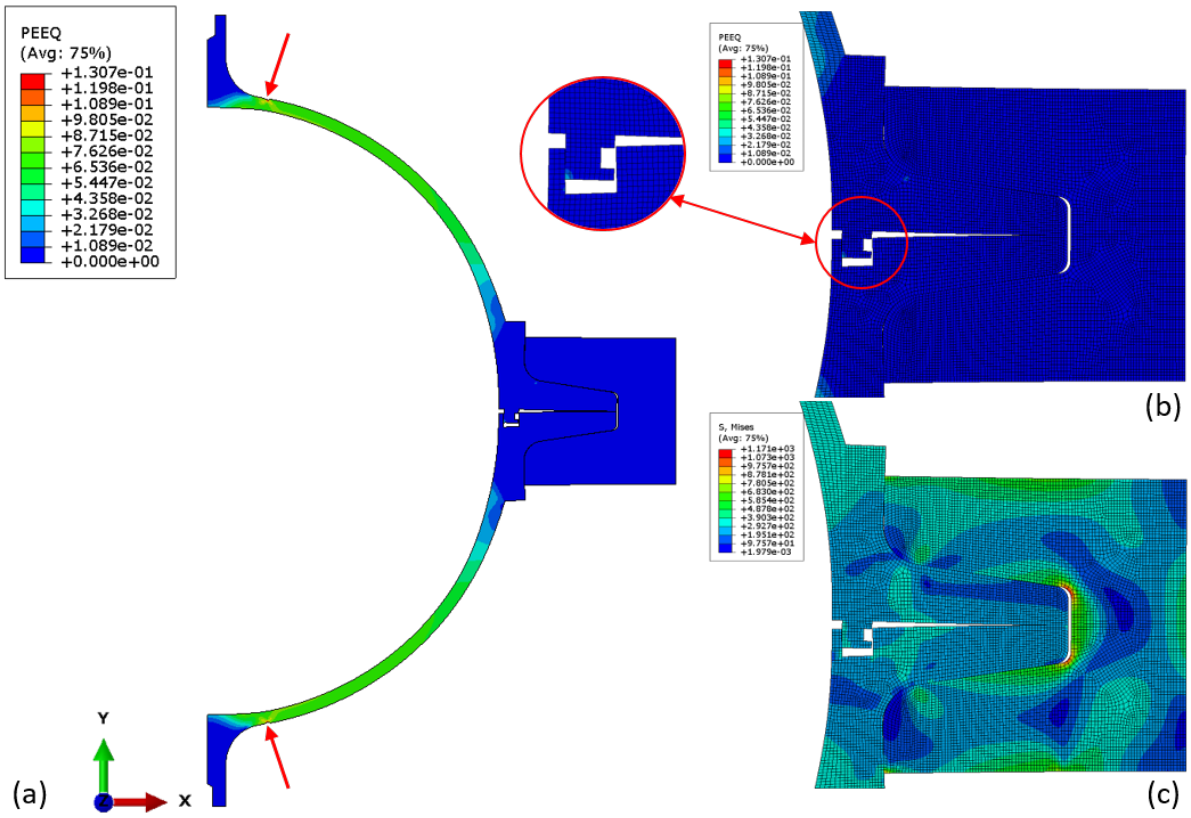

Figure 3-1: (a) Plastic equivalent strain (PEEQ) at 36 MPa (mesh hidden for clarity). The maximum strains occur at the latitudinal grooves as indicated by the red arrows. (b) A close-up view of the O-ring groove at 36 MPa internal pressure. (c) A close-up view of the Von Mises stresses at 36 MPa internal pressure.

4 Groove Design

To weaken the case while also maintaining most of its original mass, the grooves were added to the external surfaces of the upper and lower case as shown in Figure 2-1. Because the latitudinal grooves were added to the case design after the clamping joint analysis had mostly concluded, a model was made specifically for identifying the groove geometry.

4.1 Analysis

4.1.1 Thin-Walled Pressure Vessel Assumption

For an idealized thin-walled spherical pressure vessel, the tensile stress of the outer wall at an internal pressure, P, is given by Equation 1, where r is the internal radius and t is the wall thickness.

$$\sigma = \frac{Pr}{2t} \tag{1}$$

The case geometry was idealized as a spherical vessel using the internal radius and minimal thickness across the case wall. Given that the ratio of the outer diameter (D) of the case to its minimal wall thickness is significantly greater than 10 (i.e. $\frac{D}{t} \gg 10$), the thin-walled assumption was chosen to approximate the tensile stress of the vessel. The thickness of this idealized case was reduced until the tensile stress of the outer wall exceeded the UTS of the case material (SS 316 as described in Table 2-1).

4.1.2 Stress Concentration Factor

Because stress concentrations are known to form at regions such as grooves, a stress concentration factor, K_{tg}, was considered in addition to the thin-walled pressure vessel assumption. The aim was to approximate a groove geometry (depth, t, and radius, r) that would weaken the case enough to cause failure once the design pressure was exceeded. Like that of the thin-walled pressure vessel, the failure metric was defined to be when the UTS of the case material was exceeded anywhere within the model.

Because the grooves of the test assembly will be machined using a ball end mill, the groove geometry was defined using two parameters (depth and radius), both of which are depicted in Figure 4-1.

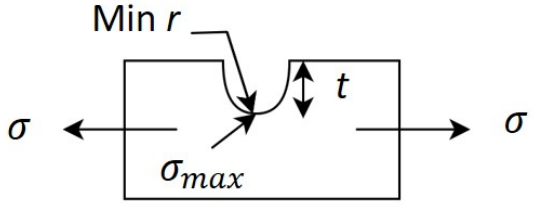

Figure 4-1: A cross-sectional view of the groove geometry, where t and r denote the groove depth and radius, respectively. Both σ and σ_{max} represent the tensile stress along the nominal case thickness and the peak stress at the groove, respectively.

Based on the contour of this groove geometry, the stress concentration factor was approximated as a function of the groove dimensions (t and r) using Equation 2, which was taken from [5] and can also be seen in Figure A-1.

$$K_{tg} = 0.855 + 2.21\sqrt{\frac{t}{r}} \tag{2}$$

The peak stress at the groove could then be estimated as a function of K_{tg} and the tensile stress along the nominal case thickness (σ) using Equation 3. Taken from [5], Equation 3 can also be seen in Figure A-1:

$$\sigma_{max} = K_{tg}\sigma \tag{3}$$

It should be noted that σ is analogous to the tensile stress approximated in Equation 1.

4.1.3 Groove Analysis Finite Element Model

Although idealizing the case as a thin-walled pressure vessel and using a stress concentration factor to approximate the groove geometry are useful preliminary tools, building a finite element model was necessary for obtaining a more accurate solution. The stress concentration factor, for example, does not account for the curvature of the case geometry. Additionally, unlike an Abaqus finite element model, neither of the aforementioned methods consider nonlinear effects. While these limited techniques were used to obtain an initial geometric configuration, the groove geometry was ultimately refined using a finite element model.

Geometry. Created in ABAQUS/CAE, the model consisted of an axisymmetric representation of a spherical vessel, using the nominal inner radius and thickness of the case subassembly. To replicate the geometry of the latitudinal grooves shown in Figure 2-1, a groove feature was added to the geometry equator as shown in Figure 4-2. To maximize the mesh quality, the geometry surrounding the groove was partitioned.

Mesh. Like that of the case assembly analysis, the pressure vessel was meshed using CAX4R elements with 16 elements across the nominal thickness (11 across the ligament[3]). Additionally, 26 elements surrounded the groove edge as shown in Figure 4-3. This highly refined mesh was used because the stress was expected to concentrate at the base of the groove, thus it was important to refine the mesh enough to capture this behavior. Though a convergence study indicated a coarser mesh would have been sufficient, the low computational cost afforded by an axisymmetric model made implementing a finer mesh possible.

Material. The material used for the model was the same as that applied to the upper and lower case components (see SS 316 in Table 2-1).

Loading and Boundary Conditions. The loading profile applied to the model was identical to that described in Section 2.4. To prevent non-physical translations, all nodes coincident with the symmetry axis were fixed in the radial direction (x-direction) as shown in Figure 4-2. Given the uniformity of the load profile, the model was not constrained axially to prevent non-uniform

[3]The ligament length is simply the nominal thickness of the pressure vessel less the groove depth.

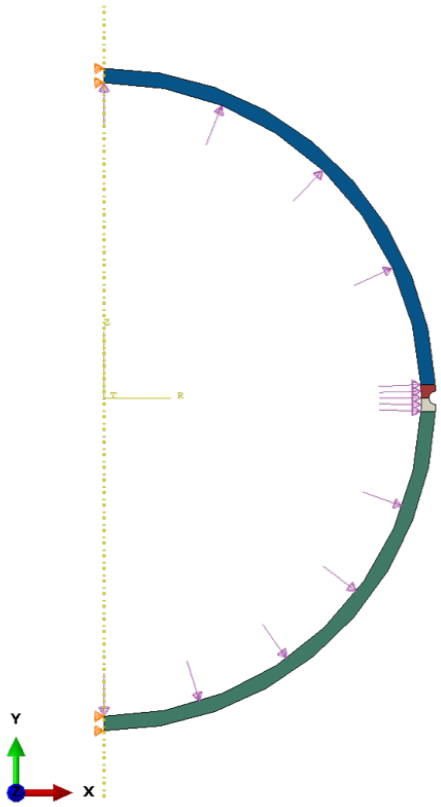

Figure 4-2: Axisymmetric model for the idealized case pressure vessel, where the different colored regions arise from partitioning. The pressure load was applied uniformly to the internal surface as indicated by the purple arrows. The nodes coincident with the symmetry axis were fixed in the radial direction (horizontal direction) as indicated by the orange triangles.

distortions. If the pressure distribution had not been radially uniform, axial constraints would have been required to converge on an accurate solution.

Analysis. Monotonically increasing internal pressure was applied to the FE model in the same manner and magnitude as described in Section 3.

Groove Design

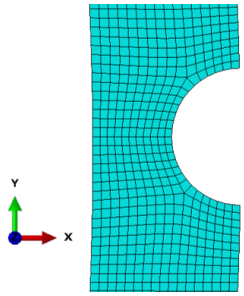

Figure 4-3: Meshed region of groove geometry.

4.2 Results

Idealizing the case geometry as a spherical vessel resulted in a nominal internal radius and wall thickness of 190 mm and 8.6 mm, respectively. To determine at what thickness the tensile stress of the outer wall would theoretically exceed the UTS of SS 316, the stress calculated from Equation 1 was plotted as a function of the wall thickness, shown in Figure 4-4.

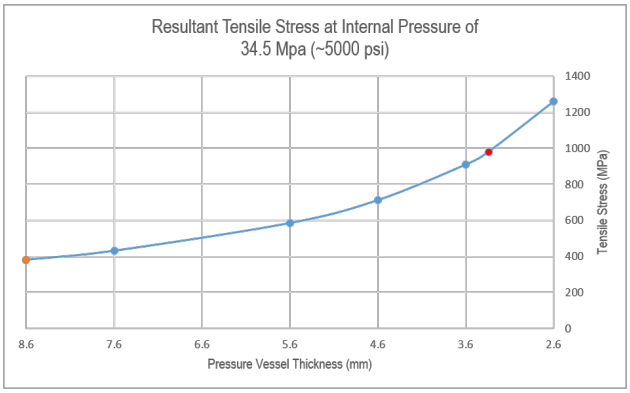

Figure 4-4: Approximating the tensile stress of a pressure vessel when subjected to an internal pressure of 34.5 MPa ($\sim$5000 psi). The orange marker denotes the resultant tensile stress at the nominal case thickness, while the red marker indicates the thickness at which the UTS of the material (SS 316) is exceeded by the resultant tensile stress.

Based on the results shown in Figure 4-4, the case would require a minimal thickness of approximately 3.3 mm to exceed the UTS of the vessel material.

Because the case would lose a significant amount of mass if this reduction in thickness was implemented, an alternative solution was to induce a high enough stress concentration within the case wall while still preserving the original mass. Thus, rounded grooves were added to the case geometry. The aforementioned calculation was used to provide an initial groove geometry estimation: a minimal thickness of 3.3 mm corresponds to a groove depth of 5.3 mm (nominal thickness of 8.6 mm less the minimal thickness of 3.3 mm). Because a ball end mill will be used to machine the grooves, the estimated groove depth was rounded to 5 mm, and 5 mm was selected as the initial groove radius. Substituting these values into Equation 2 resulted in a stress concentration factor (K_{tg}) of 3.065. Substituting this value into Equation 3 along with the predicted tensile stress (σ)

Table 4-1: Maximum pressure withstood by pressure vessel analytical model based on groove depth/radius.

Groove Radius (mm)	5	4	3	2
Groove Depth (mm)	5	4	3	2
Maximum Pressure (MPa)	28.15	34.76	40.86	45.18

given a wall thickness of 8.6 mm ($\sim$381 MPa as shown in Figure 4-4) yielded a maximum tensile stress (σ_{max}) of 1167 MPa at the groove.

Using a depth and radius of 5 mm as an initial approximation, a finite element model was used to determine if the required depth and radius of the groove could be reduced even further to preserve the mass of the case subassembly. The finite element analysis was executed using a combination of groove depths and radii. However, all used a groove depth-to-radius ratio of one given the machining process that would be used. Studies were executed at groove depths of 2, 3, 4, and 5 mm. The maximum internal pressure withstood by each model prior to model divergence was placed in Table 4-1.

Based on the design specification that the case assembly should not exceed 5000 psi (34.5 MPa) by a significant margin, Table 4-1 shows that 4 mm is the recommended groove depth and radius for the groove geometry for the upper and lower case components.

5 Conclusion

The analysis efforts performed by W-13 determined that the case design proposed by M-6 would sufficiently pressurize contents up to 5000 *psi* under quasi-static conditions. A design recommendation explicitly provided by W-13 was to add latitudinal and longitudinal grooves to the case components with groove depths and radii of 4 *mm*. The function of the grooves was to weaken the case while simultaneously maintaining its overall mass.

Appendix A: Stress Concentration Factor

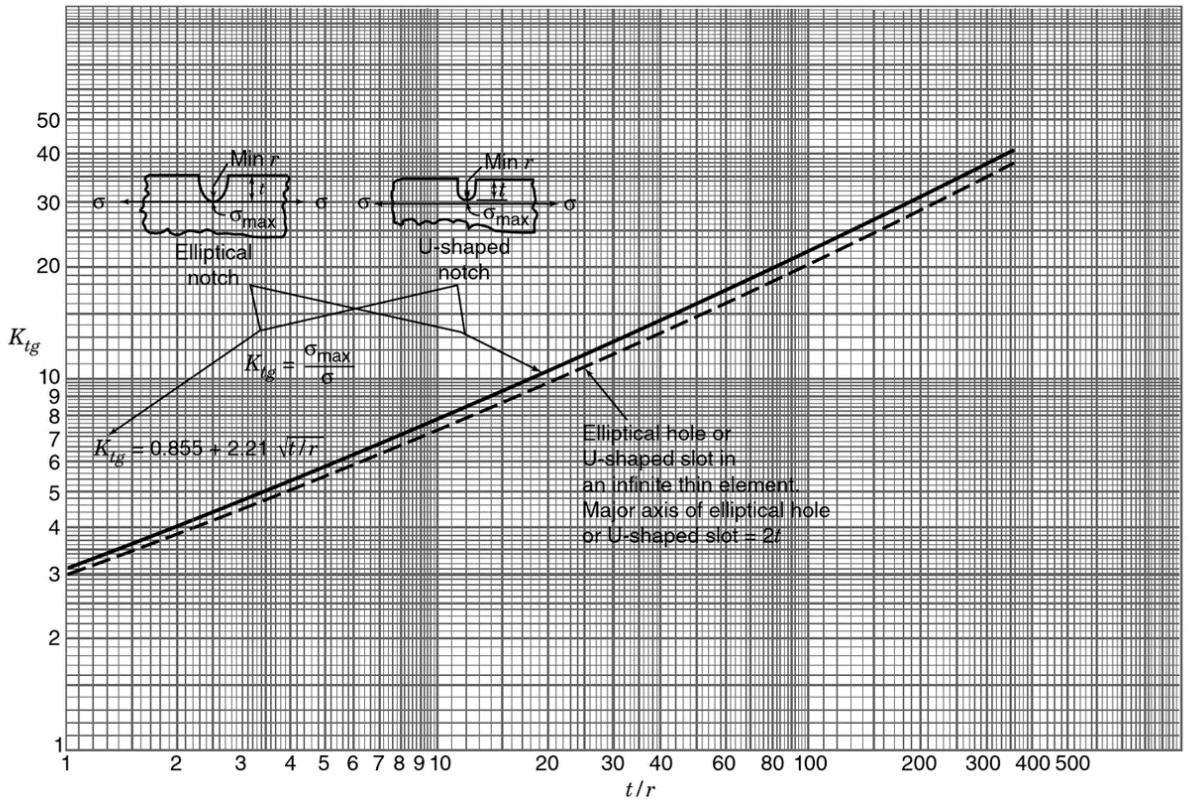

Figure A-1: Stress concentration factors K_{tg} for an elliptical or U-shaped notch in a semi-infinite thin element in tension [5]

References

[1] "17-4PH, H900, Bar, Thickness: Up to 8.001 in, AMS 5643, A Basis," V.X, Database: *MMPDS-13 Database, 1.8.1m_ June2019*, Granta Design.

[2] "Atlas of Stress-Strain Curves". In: 2nd ed. 10. Materials Park, OH: ASM International, 2002, p. 200.

[3] "Structural Alloys Handbook: 316 Stainless". In: vol. 2. West Lafayette, IN: CINDAS LLC, 1977, pp. 5, 35.

[4] J.F. Sullivan. "Technical Physics". In: Wiley, 1988, p. 204.

[5] D. F. Pilkey W. D. Pilkey and Z. Bi. "Peterson's Stress Concentration Factors". In: 4th ed. Hoboken, NJ: Wiley, 2020, p. 114.